Diagnosis of an Amplifying and Decaying Baroclinic Wave Using Wind Profiler Data

PHILLIP L. SPENCER

NOAA/National Severe Storms Laboratory, Norman, Oklahoma

FREDERICK H. CARR

School of Meteorology, University of Oklahoma, Norman, Oklahoma

CHARLES A. DOSWELL III

NOAA/National Severe Storms Laboratory, Norman, Oklahoma

(Manuscript received 25 July 1994, in final form 9 August 1995)

ABSTRACT

Kinematic and thermodynamic quantities derived from wind profiler triangles are used to help describe the structure of both an amplifying and decaying baroclinic wave as they traversed portions of the wind profiler demonstration network. The data provide excellent diagnoses of the cyclogenetic processes associated with the amplifying system and the cyclolytic processes associated with the decaying system. The importance of a baroclinic wave's vertical tilt and the associated profiler-derived advective patterns of the systems as they relate to surface evolution are shown to be consistent with conceptual models of baroclinic waves. These structural aspects of the observed baroclinic waves are also shown to vary substantially on short timescales. In addition, a subsynoptic-scale feature associated with a severe convective event that developed ahead of the decaying wave trough axis was observed quite well by the profiler network. This feature's detection was dependent on the high temporal resolution of the profiler data and was not detectable with data provided by the rawinsonde network.

1. Introduction

Our understanding of upper-air processes is limited by the spatial and temporal resolution of the upper-air observing network. Over the last several decades, the North American network has been composed mostly of twice daily rawinsonde launches from sites spaced about 400 km apart. However, since the completion of the 29-station wind profiler demonstration network (WPDN) across the central United States in 1992, accurate wind measurements throughout the depth of the troposphere at sites with an average spacing of roughly 270 km are available on an *hourly* basis. This provides high temporal and vertical resolution diagnoses of trough and ridge passages, upslope and downslope wind events along the Rocky Mountains, low-level jets, and jet streaks, just to name a few phenomena. Not only does the profiler network allow us to diagnose these processes in unprecedented detail, but the hourly observations allow temporal continuity to be introduced into upper-air analyses of important mesoscale features.

Corresponding author address: Phillip L. Spencer, National Severe Storms Laboratory, 1313 Halley Circle, Norman, OK 73069.

It has been suggested from the beginning of VHF–UHF wind profiling of the troposphere (Gage and Balsey 1978) that the resulting data would yield new insight into the spatial and temporal structure of synoptic and mesoscale phenomena (e.g., Larsen and Röttger 1982). As tropospheric profiling radars were installed, early studies (e.g., Shapiro et al. 1984) showed how the hourly wind profiles could accurately portray frontal and jet streak evolution. Augustine and Zipser (1987) provided examples of the value of wind profiler data in detailing the mesoscale structure of squall lines. When clusters of three or more profilers became available, they allowed for the computation of kinematic quantities that provided additional insight into tropospheric behavior (e.g., Zamora et al. 1987; Carlson and Forbes 1989). The use of wind profiler data to deduce thermal structure was explored by Neiman and Shapiro (1989), Hermes (1991), and, using simulated model data, Kuo et al. (1987). Although some success was noted, the studies indicated that all of the techniques utilized yielded poor estimates in rapidly evolving situations. Neiman et al. (1992) showed how a combination of wind profiler and radio acoustic sounding system (RASS) observations can diagnose lower- and midtropospheric kinematic and thermal structure. More recently, using the method of Cram et al. (1991), Karyampudi et al. (1995) derived gridded fields of wind

components, temperature, and geopotential heights, which were used to derive other diagnostic fields for the purpose of studying the mesoscale vertical structure of an upper-level jet stream and a developing tropopause fold.

In this paper, wind profiler data only are used to diagnose the kinematic and dynamical structure and evolution of mid- and upper-tropospheric baroclinic waves. Of particular focus here is the information provided by profilers on the vertical tilt of these waves and whether this tilt is consistent with subsequent surface behavior. Interpretation of the classical 3D wave cyclone model (e.g., Petterssen 1956, p. 320) indicates that troughs tilting upstream with height are conducive to surface low development, while downstream tilts lead to surface low decay. This is also in agreement with quasigeostrophic (QG) theory, which provides guidance on which horizontal and vertical vorticity and temperature distributions are associated with cyclogenetic and cyclolytic behavior (e.g., Holton 1992, p. 239). It is shown that the vorticity and temperature advection patterns estimated from profiler data are consistent with observed surface development.

We examine two synoptic cases, the first an amplifying wave case during 7–8 October 1992, and the second a decaying wave case during 2–3 April 1991. The April 1991 case also provides an example of a "mesowave," an upper-level trough detected by all four of the Oklahoma profilers that was completely missed by the rawinsonde network. In section 2 we briefly describe the profiler data, the analysis techniques applied to the data, and how the various kinematic and thermodynamic variables are derived. In sections 3 and 4, respectively, we use triangle calculations to examine the kinematic and thermodynamic structure of the amplifying and decaying baroclinic waves. Section 5 focuses on a severe convective event and the associated mesoscale short-wave trough that preceded the decaying wave trough axis. Finally, section 6 contains a brief summary and concluding remarks.

2. Data and analysis methods

The data used to examine the amplifying system of 7–8 October 1992 are from the profilers located near Purcell, Oklahoma (PRCO), Haviland, Kansas (HVLK), and Neodesha, Kansas (NDSK) (See Fig. 1). The four Oklahoma profilers (VCIO, LMNO, HKLO, and PRCO) form two nearly equilateral triangles that are used to diagnose the decaying system of 2–3 April 1991.

Six-minute radial velocity data from the wind profilers are transmitted to the profiler hub in Boulder, Colorado, where the data are processed and archived (Barth et al. 1994). A consensus averaging technique (Strauch et al. 1984) and preliminary quality control are performed at the Hub to yield hourly wind estimates from 500 to 16 250 m AGL, in increments of 250 m.

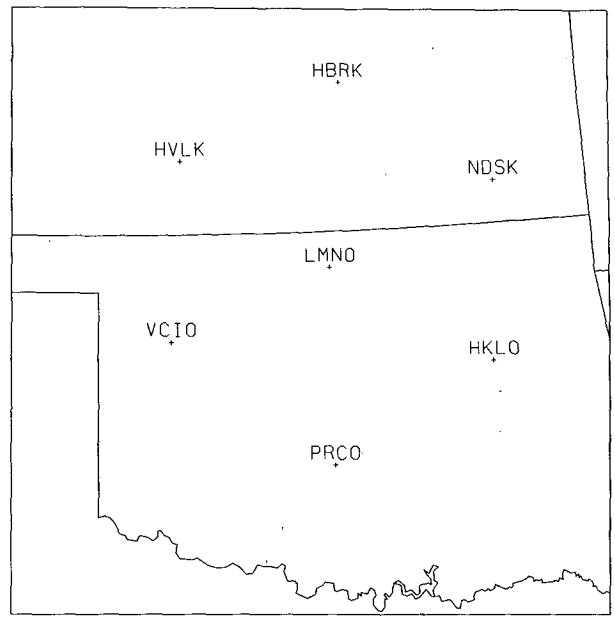

FIG. 1. Oklahoma and Kansas wind profiler demonstration network sites.

In addition, we implement median and shear checks similar to those used by Brewster and Schlatter (1986) that are used to rid the data of erroneous and unrepresentative data. The median check compares the horizontal wind components of each datum to the median of each component of a set of neighbors within the time–height section. If the difference in either component exceeds a threshold, then the datum is eliminated. The shear check seeks to eliminate those data within each profile that are responsible for excessive directional or speed shear. A more complete description of the quality-control scheme is found in Carr et al. (1995, hereafter CSDP95). Strauch et al. (1987), Weber and Wuertz (1990), and Weber et al. (1990) discuss the accuracy of profiler winds.

A distance-dependent weighted averaging objective analysis scheme suitable for time–height data is then applied to the quality-controlled data. The chosen scheme is similar to that presented by Doswell (1977) in which a datum's influence upon a gridpoint value is related to both its spatial and temporal separation from the grid point. This low-pass analysis scheme, described in greater detail by CSDP95, not only produces a regular time–height grid at each of the three stations (1 h × 200 m resolution grid) but allows us to filter the data to remove unwanted scales. We have chosen the weight function parameters such that the retained amplitude of the Nyquist wavelength and period is essentially zero. (See the short-dashed curve in Fig. 1 of CSDP95.) Using nearby sounding data, these height-coordinate winds are interpolated onto pressure surfaces (10-mb increment) using a linear scheme. The

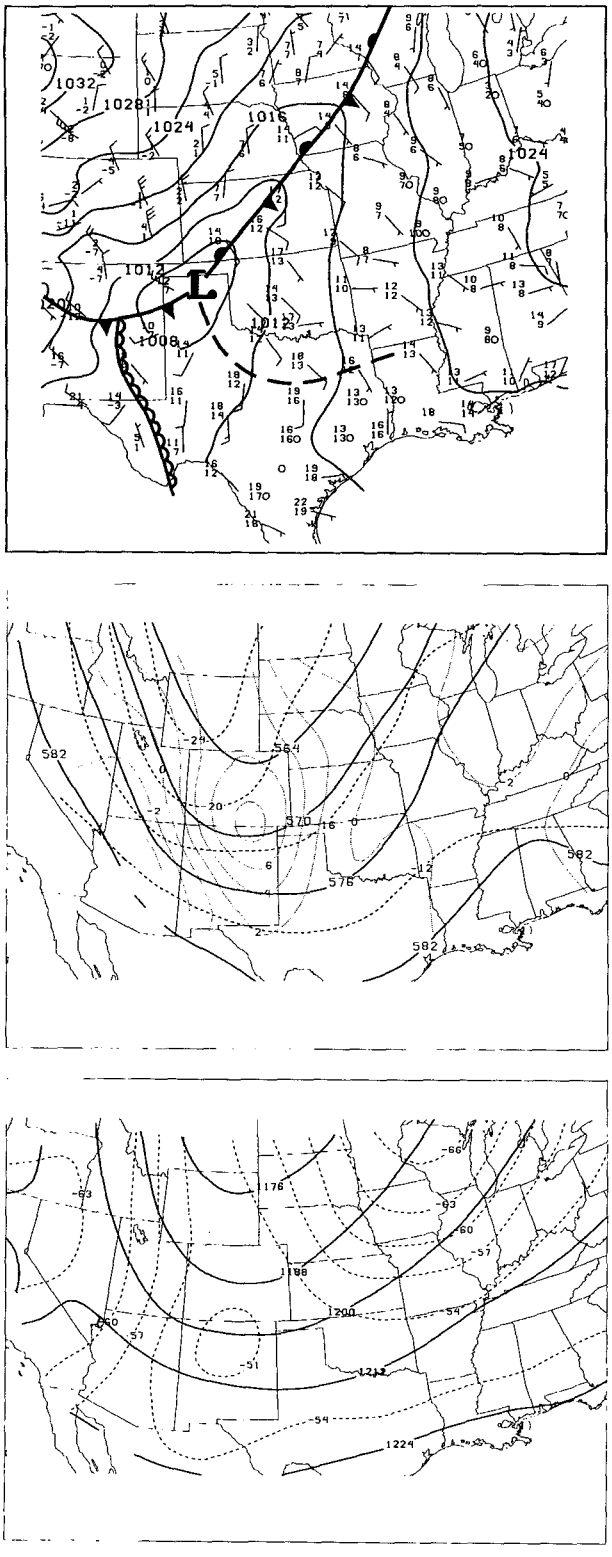

FIG. 2. GEMPAK analyses (see Koch et al. 1983) valid at 1200 UTC 7 October 1992: (a) surface pressure (every 4 mb); (b) 500-mb heights (solid lines, every 6 dam), temperature (dashed lines, every 4°C), and vorticity ($\times 10^5$, dotted lines, every 2 s^{-1}); and (c) 200-mb heights (solid lines, every 12 dam) and temperature (dashed lines, every 3°C).

"linear vector point function (LVPF)" method (Doswell and Caracena 1988; Zamora et al. 1987), modified to include the effects of earth curvature (CSDP95), is used to calculate kinematic fields (including divergence and vorticity) from a set of stations (here, a triangle with the stations at the vertices). We perform the diagnostic calculations up to about 180 mb, a height slightly above the tropopause.

The LVPF method for calculating kinematic quantities is used in this study for two reasons. First, the 2–3 April 1991 event occurred during the early portion of the WPDN installation period when only a few profilers were operating, thus excluding the possibility of performing objective analysis over a substantial domain. To be consistent, the 7–8 October 1992 case is evaluated using the same technique. Second, Schaefer and Doswell (1979) and Doswell and Caracena (1988) showed that calculating divergence and vorticity directly from randomly spaced wind observations produces more accurate results than the conventional method of derivative estimation from a uniform array of gridded observations. Both Davies-Jones (1993) and Zamora et al. (1994) have recently discussed the errors associated with line integral methods using profiler data. Lee and Browning (1994) also did an extensive analysis of divergence and vertical motion errors from the kinematic technique. These analyses need not be repeated here. According to the Zamora et al. analysis, the minimum wavelength for study by the Oklahoma–Kansas profilers is 600 km, while the temporal scale (for hourly sampling intervals and sampling errors less than 10%) needs to be at least 18 h. Both of these criteria are satisfied for the ampli-

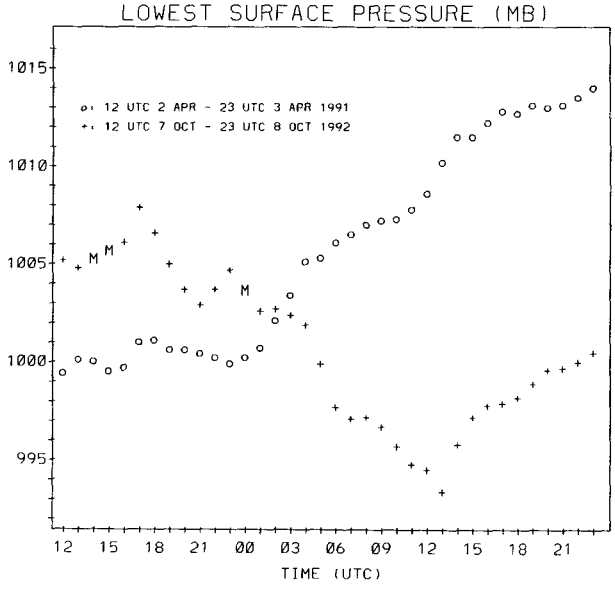

FIG. 3. Lowest surface pressure of the 7–8 October 1992 system (+) for the period 1200 UTC 7 October–2300 UTC 8 October and of the 2–3 April 1991 system (O) for the period 1200 UTC 2 April–2300 UTC 3 April. Time increases from left to right.

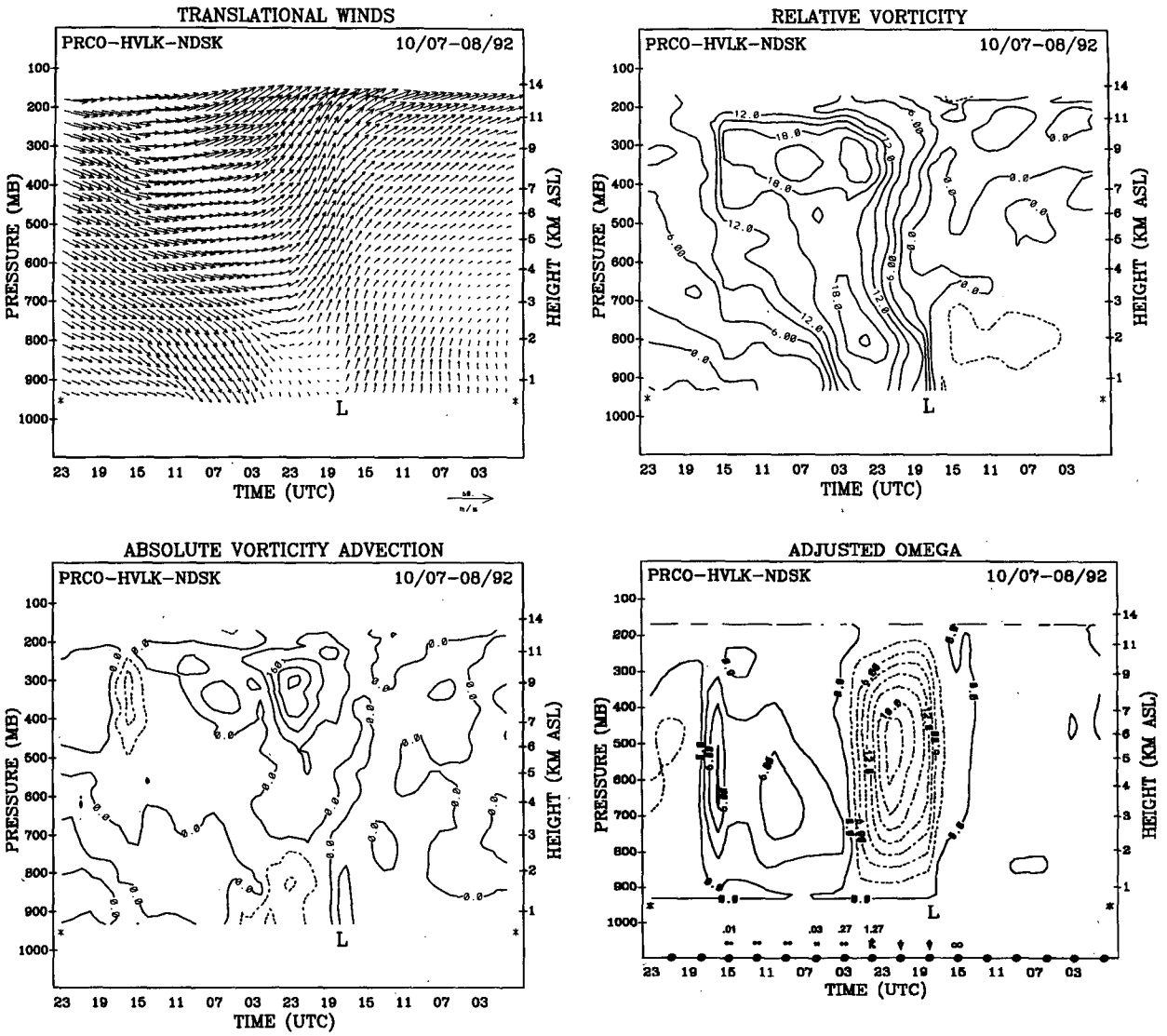

FIG. 4. PRCO–HVLK–NDSK profiler triangle calculations for 7–8 October 1992 of (a) translational winds, (b) relative vorticity ($\times 10^5$; contour interval of 3 s^{-1}), (c) absolute vorticity advection (contour interval of 80 s^{-1} day^{-1}), (d) vertical motion (adjusted kinematic omega; contour interval of 3 $\mu b\ s^{-1}$), (e) adjusted divergence ($\times 10^5$; contour interval of 2 s^{-1}), and (f) virtual temperature advection by the translational wind (contour interval of 0.3° h^{-1}). Time increases from right to left. Dashed contours are negative values. Surface trough passage is indicated by the "L". Asterisk indicates centroid elevation. Three-hourly accumulated precipitation, current weather, and cloud cover for ICT, which lies near the northern edge of the triangle, are also plotted on (d).

fying and decaying wave cases; for the "mesowave" case discussed in section 5, the relative divergence error will approach 20%. The expected error in the actual divergence estimates is on the order of 1×10^{-5} s^{-1}.

Given the time–height section of divergence derived from the LVPF method, the pressure-coordinate form of the mass continuity equation is integrated to find vertical velocity ω. A linear adjustment procedure, which assumes that errors in the divergence are independent of pressure and that the vertical velocity is zero at both the top and bottom of the domain, is applied to yield physically acceptable values of vertical velocity. (All subsequent discussions involving divergence refer to the adjusted divergence field; that is, the divergence field that, when integrated, produces the adjusted vertical velocity field. The wind fields remain unadjusted.)

The vorticity equation in the form

$$-\mathbf{V}_H \cdot \nabla(\zeta + f) = (\zeta + f)\delta + \frac{\partial \zeta}{\partial t}, \qquad (1)$$

where $\mathbf{V}_H$ is the horizontal wind vector, ζ the relative vorticity, f the Coriolis parameter, δ the divergence, and t time, is used to estimate the hourly horizontal

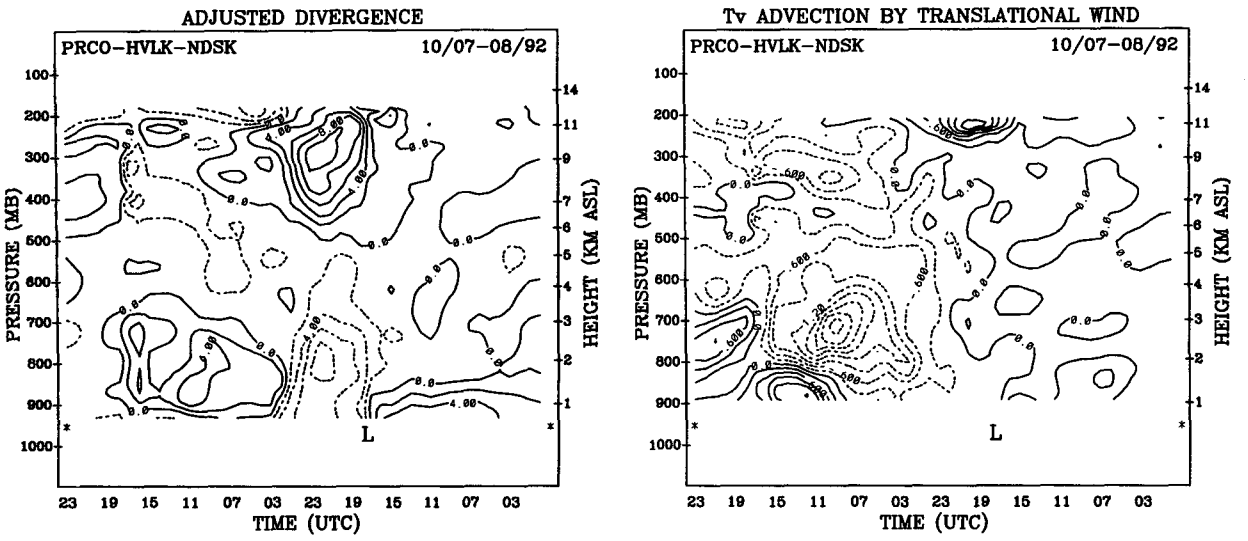

FIG. 4. (*Continued*)

absolute vorticity advection at each pressure level. This is essentially the quasigeostrophic vorticity equation except that we retain relative vorticity in the divergence term since it is of order f in the troughs under study and we use our kinematic estimates of relative vorticity rather than geostrophic vorticity. The neglect of friction requires that we limit our interpretation of the vorticity advection patterns to the mid and upper troposphere. Also, we employed time-to-space conversion to estimate the magnitude of the tilting term and found that even though large "horizontal" gradients of vertical velocity were present in portions of the time series, they were coincident with very small or negligible vertical wind shear, resulting in a tilting term contribution to horizontal vorticity advection that was much smaller than the contribution of the divergence term. Thus, for our applications, neglecting the tilting term appears to be justified. Centered finite-difference calculations are applied to find the temporal variation of relative vorticity. The latitude of the triangle centroid is used in the computation of the Coriolis parameter.

In order to obtain information about the thermodynamic structure of the baroclinic waves, the thermal wind equation in the form

$$\frac{\partial \mathbf{V}_g}{\partial p} = -\frac{R_d}{fp}\mathbf{k} \times \nabla T_v, \qquad (2)$$

where $\mathbf{V}_g$ is the geostrophic wind vector, p is pressure, R_d the gas constant for dry air, and T_v the virtual temperature, is used to estimate the horizontal virtual temperature gradient. For the cases studied, the geostrophic wind field, derived following the method of Zamora et al. (1987), appeared to be somewhat unrealistic (magnitudes greater than 100 m s^{-1} at times) when compared to typical synoptic- and subsynoptic-scale analysis values. Neiman and Shapiro (1989), as well, found that "details within the derived field [of geostrophic winds] were highly questionable." For this reason, we have substituted the translational wind field (which approximates the mean wind in the triangle) in place of the geostrophic wind field in (2). This substitution is most valid above the boundary layer where the translational wind more likely resembles the true geostrophic wind. Having an estimate of the temperature gradient, we calculate a virtual temperature advection field, where the translational wind is combined with the inferred temperature gradient information.

3. Amplifying wave

a. Weather summary

Analyses for 1200 UTC 7 October 1992 (Fig. 2) reveal that a surface low pressure center has developed and is located in the Texas panhandle on a frontal boundary that extends northeastward to the Great Lakes region. Aloft (Figs. 2b,c), a negatively tilted shortwave trough approaches the Great Plains states from the west. The temperature contrast along the front increases dramatically during the morning as the front moves southeastward. Severe thunderstorms develop along the rapidly moving cold front during the afternoon from eastern Oklahoma southwestward toward the Big Bend area of southwest Texas. Rapid cyclogenesis occurs as the upper trough forms a closed low over the central Plains. The northeastward-moving surface low reaches its lowest pressure of 993 mb (Fig. 3) in southwestern Iowa during the morning of 8 October and by the afternoon hours has created an impressive spiral cloud band. The surface low begins to fill during the late morning and afternoon hours of 8

October as the system loses its upstream vertical tilt. Evening (0000 UTC 9 October) analyses (not shown) indicate that the system has acquired a slight downstream vertical tilt over Iowa.

b. Profiler calculations

The translational winds valid at the PRCO–HVLK–NDSK centroid (hereafter, P–H–N; Fig. 4a) reveal the passage of a low-level trough near 1800 UTC 7 October 1992. Trough passage at higher levels occurs at increasingly later times, implying that the trough has an upstream tilt with height. Strong south and southwesterly winds precede the passage of the trough axis, with northwesterly winds following trough axis passage. The consistency of this tilt in the time–height domain (0.01 mb s^{-1} between 850 and 300 mb) can be checked with the spatial tilt estimated from synoptic charts (91 mb per 100 km) with the use of the system advective velocity during 8 October. The observed value of 8 m s^{-1} yields a slope of 125 mb per 100 km.

The P–H–N vorticity field (Fig. 4b) is dominated, unsurprisingly, by the high values (21×10^{-5} s^{-1}) of vorticity associated with the trough axis. Note how the strong curvature along the upstream-tilted trough axis produces an upstream tilt in the vorticity field. These high values of vorticity at lower pressures positioned upstream from the surface low provide a favorable situation for surface development. Intensification commences as the high upper-level vorticity values are advected over the downstream surface low, creating a situation in which cyclonic vorticity advection increases with height. Indeed, the P–H–N absolute vorticity advection (Fig. 4c) and derived differential cyclonic vorticity advection (DCVA; not shown) fields indicate the presence of strong positive DCVA during the development phase of the surface low. Recall that via the quasigeostrophic ω equation, positive values of DCVA provide a positive contribution to rising motion. A comparison of the vertical gradients of absolute vorticity advection in Fig. 4c with the omega field (Fig. 4d) derived as described in section 2 shows nearly perfect correspondence for the rising motion maximum near 2200 UTC 7 October and the sinking motion maximum at 1600 UTC 8 October. Thus, there is excellent consistency between implied quasigeostrophic forcing and kinematic omegas from profiler data.

The divergence field (Fig. 4e) associated with the upward vertical motion pattern shown in Fig. 4d plays a vital role in the atmosphere's attempt to maintain the upstream vertical tilt of the system. Holton (1992, p. 239) describes how a westward-tilting system is able to maintain its tilt despite the fact that given a large westerly thermal wind component, the vorticity advection patterns favor the upper wave racing ahead of the lower wave. The simple two-level model theory that he describes attributes the maintenance of the vertical tilt of a trough to secondary circulations that are associated with downstream rising motion resulting from positive DCVA. In particular, upward vertical motions ahead of the trough tend to slow down the advective tendencies of the upper wave by decreasing the time rate of change of vorticity via divergence while tending to speed up the advective tendencies of the lower wave by increasing the time rate of change of vorticity via convergence, thus keeping the upper and lower waves in step with each other.

These relationships can be expressed mathematically in a rather straightforward fashion. Consider (1) rewritten as

$$\frac{\partial \zeta}{\partial t} = -\mathbf{V}_H \cdot \nabla(\zeta + f) - (\zeta + f)\delta. \qquad (3)$$

If the lower wave (denoted by subscript l) is to stay in phase with the upper wave (denoted by subscript u), then

$$\left(\frac{\partial \zeta}{\partial t}\right)_l = \left(\frac{\partial \zeta}{\partial t}\right)_u. \qquad (4)$$

For a baroclinic atmosphere, $[-\mathbf{V}_H \cdot \nabla(\zeta + f)]_u$ usually exceeds $[-\mathbf{V}_H \cdot \nabla(\zeta + f)]_l$, so that in order for (4) to be satisfied, $[-(\zeta + f)\delta]_l > [-(\zeta + f)\delta]_u$. This condition is always true in an inertially stable atmosphere ($\zeta + f > 0$), where $\delta_l < 0$ and $\delta_u > 0$. The upper-tropospheric divergence and the lower-tropospheric convergence ahead of the trough axis, as shown in Fig. 4e, agree well with this simple model of the atmosphere's maintenance of the westward tilt of this system.

The low-level temperature advection pattern (Fig. 4f) is also consistent with the westward tilt of the system. Specifically, the low-level cold advection to the west of the surface low hydrostatically lowers midtropospheric heights in that region (and raises surface pressure), while low-level warm advection to the east of the surface low hydrostatically raises midtropospheric heights in that area (and lowers surface pressure).

The strong warm thermal advection near 200 mb slightly upstream of the surface low is consistent with upper-level warming associated with a tropopause undulation. This pattern [also evident on each of the single-station thermal advection patterns derived following the procedure of Neiman and Shapiro (1989)] compares quite favorably to NMC analyses (not shown), which indicate upper-level warm thermal advection at P–H–N during the morning of 7 October until just after 0000 UTC 8 October. (One can anticipate this warm advection by noting the large 200-mb warm pool over New Mexico at 1200 UTC 7 October evident in Fig. 2c.) Hirschberg and Fritsch (1991) discuss the significance of a warm stratospheric pool of air as it relates to intensity changes in a wave cyclone. In particular, using hydrostatic arguments they show that in a baro-

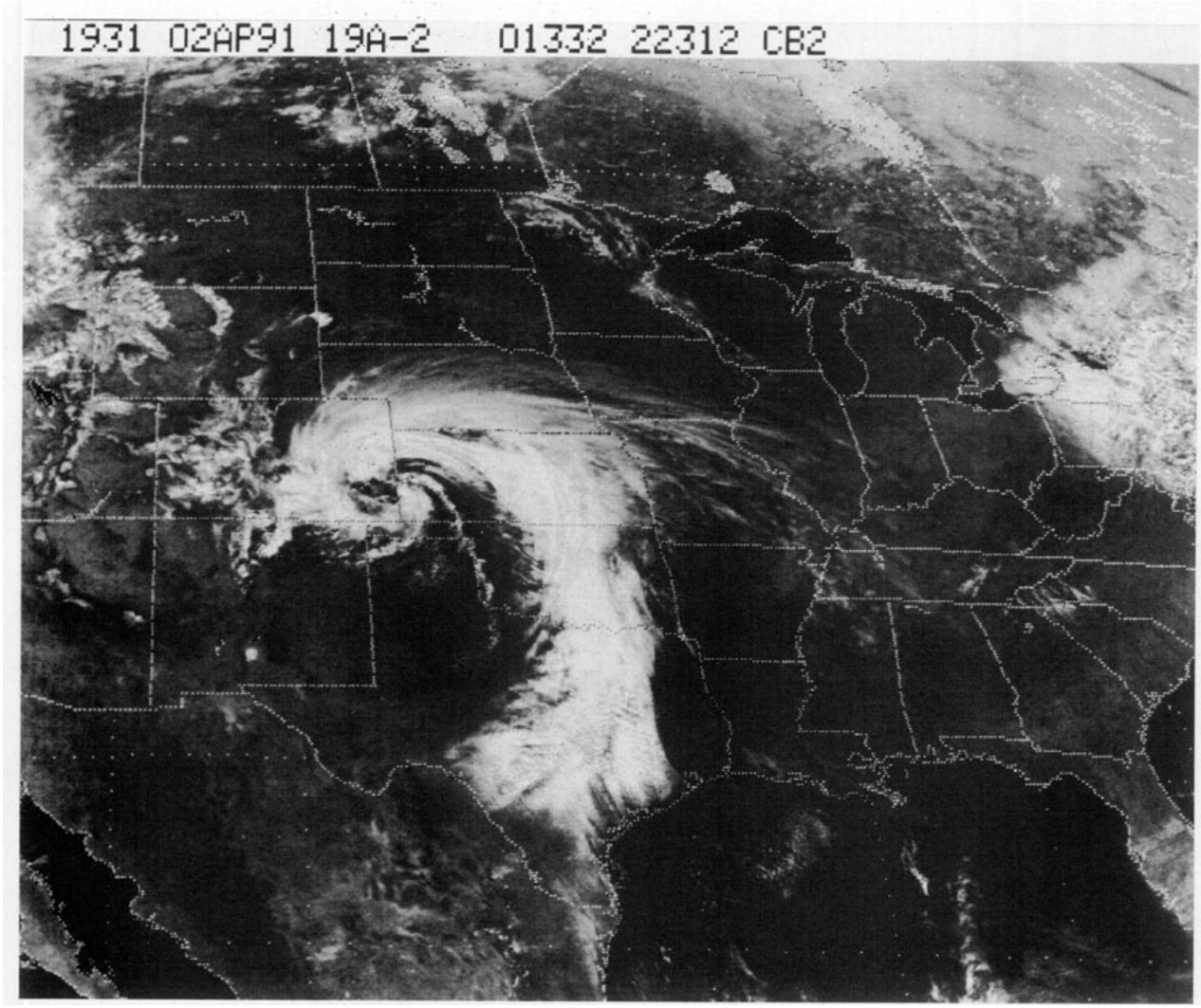

FIG. 5. Visible satellite imagery for 1931 UTC 2 April 1991.

clinic atmosphere, surface pressure responds to upper-level temperature changes much more than to an equivalent mid- or lower-tropospheric temperature change. The subsequent synergistic interaction between the upper and lower levels can intensify the surface low as long as the system maintains a westward vertical tilt. Viewed another way (e.g., Boyle and Bosart 1986), the advection of warm stratospheric air produces a region in which thermal advection increases with height. This differential thermal advection leads to height falls which, in turn, force vorticity production. Upper-level vorticity then is advected downstream over the surface cyclone, leading to pressure falls. Figure 4f shows that the thermal advection maximum near 200 mb, lying over near zero values in the mid- and lower troposphere, is well-positioned to contribute to the development of the 7–8 October cyclone.

4. Decaying wave

a. Weather summary

Analyses for 1200 UTC 2 April 1991 (not shown) reveal that a westward tilted trough is in the process of crossing the Rocky Mountains. The low-level trough is in eastern Colorado and the upper-level trough is over the western portion of the state. Surface ridging along the Texas coast shifts northeastward, allowing gulf moisture to begin its return toward the western half of Oklahoma. Surface dewpoint temperatures along the coast at this time are near 16°C, while only about 6°C throughout northern Texas and Oklahoma. However, moisture begins to make a rapid return in response to the strengthening low-level pressure gradient. Early afternoon visible satellite imagery (Fig. 5) indicates that a band of clouds extends from southcentral Texas through Oklahoma and Kansas and then wraps west-

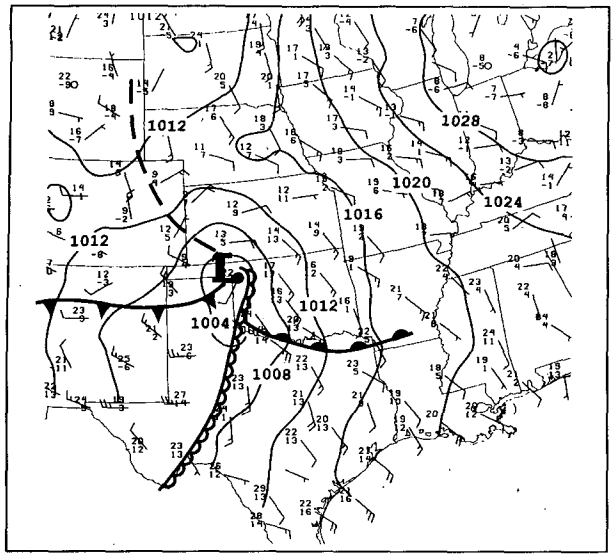

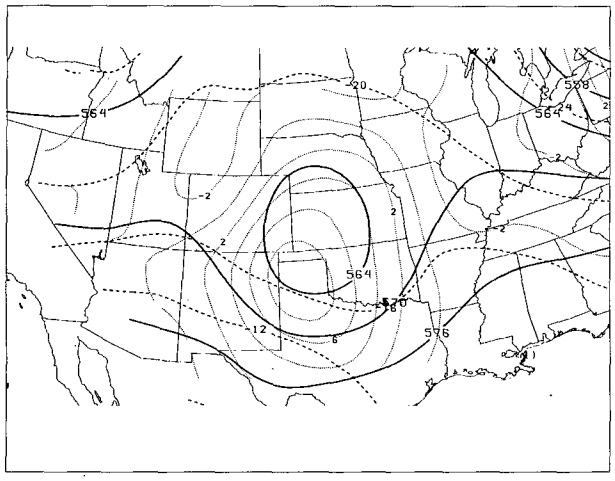

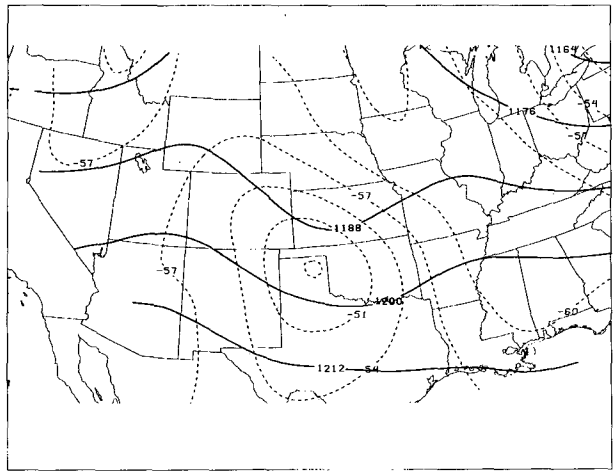

FIG. 6. Same as Fig. 2 except for 0000 UTC 3 April 1991.

ward into eastern Colorado, forming a comma-cloud pattern. The satellite photo also shows a line of towering cumulus developing in the clear region (such "dry-slot convection" has been studied previously by Carr and Millard 1985) along the western Oklahoma–Texas border northward into southwest Kansas. This line of cumulus is developing along the dryline (Fig. 6a), which extends south of the fully developed surface low. The convection rapidly intensifies to severe limits over portions of western and southern Oklahoma (Fig. 7). By 0000 UTC 3 April, the vertical tilt of the low approaches zero (Fig. 6).

The 1200 UTC 3 April analyses (not shown) reveal that the surface low is positioned over central Oklahoma, the 500-mb low over south-central Kansas, and the 300-mb trough axis over Missouri, thereby giving the weakening system a marked downstream tilt with height. Figure 3 shows that the central pressure of the surface low has risen about 8 mb since 0000 UTC 3 April. Radar summaries (not shown) reveal the rain moving out of the northeastern Oklahoma counties just after noon. However, extensive cloudiness persists throughout the day over much of the state. Lower-tropospheric cold advection overspreads the entire state during the day as the weakening system exits.

b. Profiler calculations

To investigate the decaying system of 2–3 April 1991, we examine fields derived from two Oklahoma profiler triangles. The western triangle incorporates data from the Vici (VCIO), Lamont (LMNO), and Purcell (PRCO) profilers, while the eastern triangle incorporates data from the Lamont, Haskell (HKLO), and Purcell profilers (Fig. 1). Triangle calculations again are valid at the triangle centroids, which we call V–L–P and L–H–P, for the western and eastern triangles, respectively.

Recall that Figs. 3 and 6 show that as this system's vertical tilt disappeared near 0000 UTC 3 April, the surface low development ceased. The V–L–P translational wind field (Fig. 8a) reveals that by the time the system passes through the western triangle, it has begun to acquire a slight downstream tilt with height. The low-level trough passes V–L–P at 1100 UTC 3 April, whereas the mid- and upper-tropospheric trough passes 2–3 h earlier.

The V–L–P vorticity field (Fig. 8b) associated with the trough reveals that the upper-level vorticity maximum (32×10^{-5} s^{-1}) is slightly downstream of the surface trough, as is the upper-level divergence maximum (Fig. 8e). Figure 8c indicates that zero to slightly negative differential absolute vorticity advection is occurring over the surface low as it passes through the western triangle. Also, no significant thermal advection is occurring near the low at this time (Fig. 8f), although low-level warm thermal advection precedes the low by about 8–12 h. Again, Fig. 8f indicates strong upper-

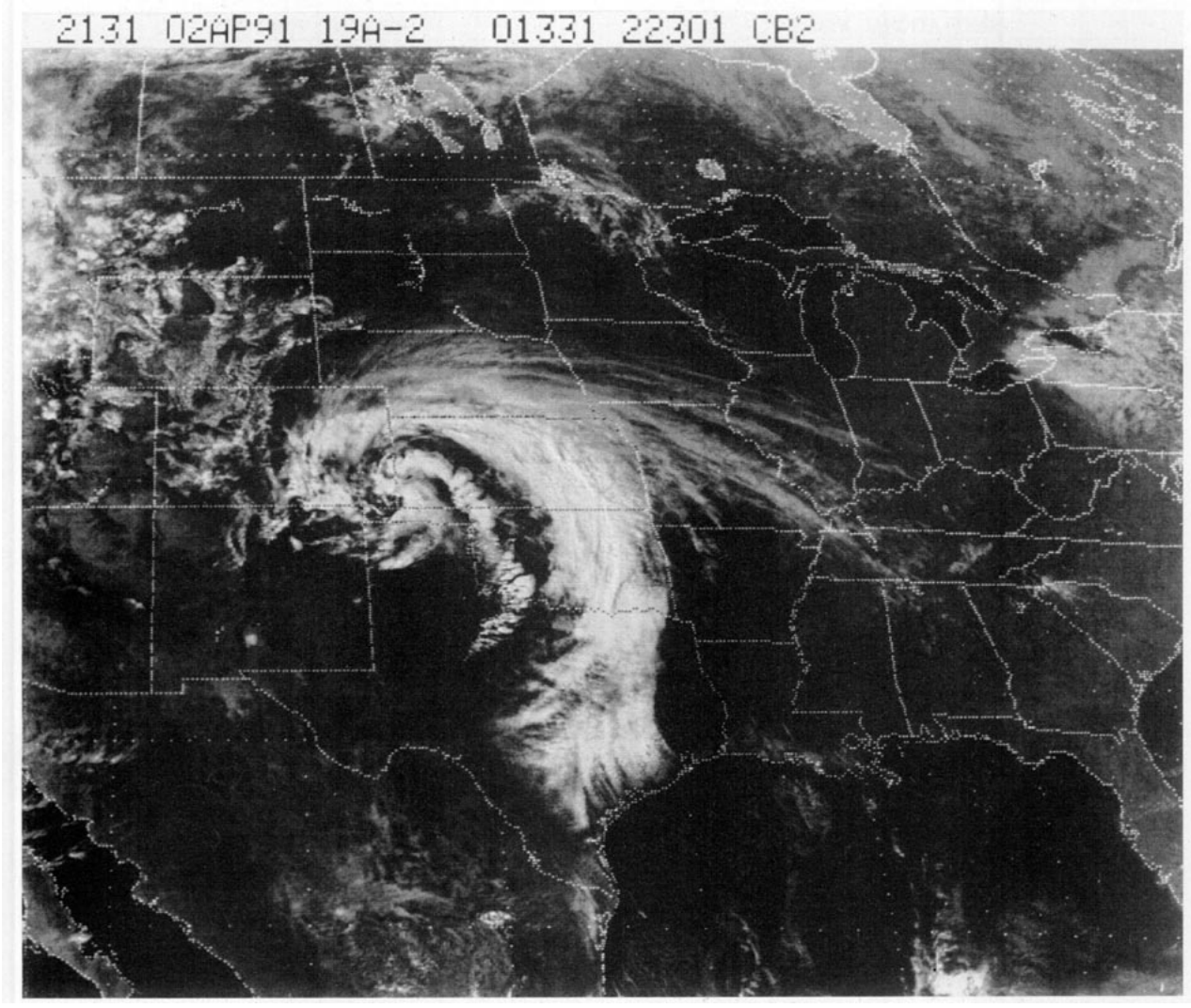

FIG. 7. Same as Fig. 5 except for 2131 UTC.

level warm advection near the tropopause (consistent with Figs. 6c and 9), but this appears to be too far downstream to have any deepening effect on the surface low. The vertical motion field (Fig. 8d) shows weak rising motion occurring over the surface low as it passes V–L–P. (These figures also reveal the presence of an upper-level feature downstream of the primary trough axis. This precursory feature and its significance are the focus of section 5.) Thus, Figs. 8a–f show that the slight downstream tilt of the system positions those advective patterns favoring cyclogenesis (i.e., positive DCVA and upper-level warm thermal advection) somewhat downstream, leaving the surface low beneath a region of weak advective patterns.

As the system moves into eastern Oklahoma, changes in these advective patterns become apparent. The L–H–P translational winds (Fig. 10a) show surface trough passage near 1500 UTC 3 April. Mid- and upper-tropospheric trough passage occurs 4–6 h earlier. Thus, the slight downstream tilt that the system had begun to acquire in the V–L–P triangle becomes even greater as it passes L–H–P.

The L–H–P vorticity field (Fig. 10b) reflects the increased downstream tilt of the system, since the upper-level vorticity maximum ($22 \times 10^{-5}\ s^{-1}$) is now 3–4 h downstream of the surface low. Therefore, instead of the highest values of midtropospheric vorticity being positioned upstream from the surface trough, providing a favorable situation for surface development (as in the 7–8 October 1992 system), or even being positioned above the surface trough (as in the V–L–P triangle), providing a neutral situation for surface development, the downstream vertical tilt provides an *un*favorable situation for surface development by promoting subsidence over the surface low via negative DCVA. The L–H–P absolute vorticity advection field

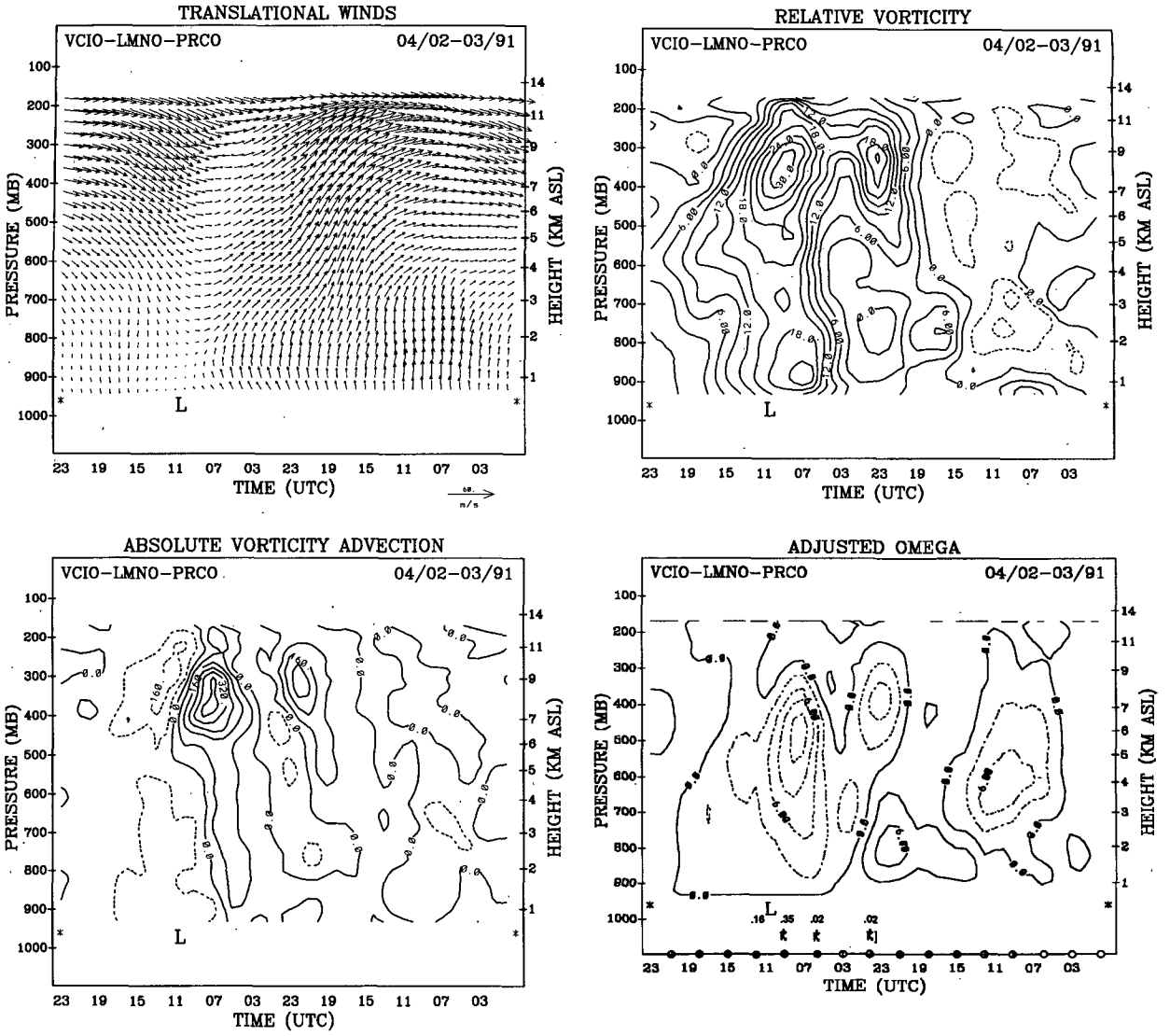

FIG. 8. Same as Fig. 4 except for the VCIO–LMNO–PRCO triangle for 2–3 April 1991. Weather information on Fig. 8d is for OKC, which lies near the eastern edge of the triangle.

(Fig. 10c) indeed shows that the strong positive DCVA is well downstream, leaving the surface low in an area mostly dominated by weak negative DCVA and subsidence (Fig. 10d), leading to surface pressure rises (Fig. 3).

Strong upper-level divergence, coupled with strong low-level convergence (Fig. 10e), continues ahead of the surface low, indicating the atmosphere's attempt to develop the low farther eastward. The increased downstream tilt of the system, however, indicates that the advective tendencies are dominating the secondary circulation. Figure 10f reveals that as the system passes through the eastern triangle and acquires an increased downstream tilt, the upper-level warm thermal advection has shifted farther downstream relative to the surface cyclone. This leaves the surface low beneath an area dominated by upper-level cold thermal advection, which contributes to cyclolysis.

5. Dry-slot convection during 2–3 April 1991

In addition to diagnosing the structure of the decaying wave, wind profiler data are used to study the conditions prior to the severe convective event of 2–3 April 1991. The high temporal resolution offered by the profilers allows for the diagnosis of an important feature (unresolvable by the rawinsonde network) that was associated with the convection. Our analysis will concentrate on the VCIO–LMNO–PRCO triangle.

The Purcell pressure-coordinate winds (Fig. 11) reveal (as do the other Oklahoma profilers; not shown)

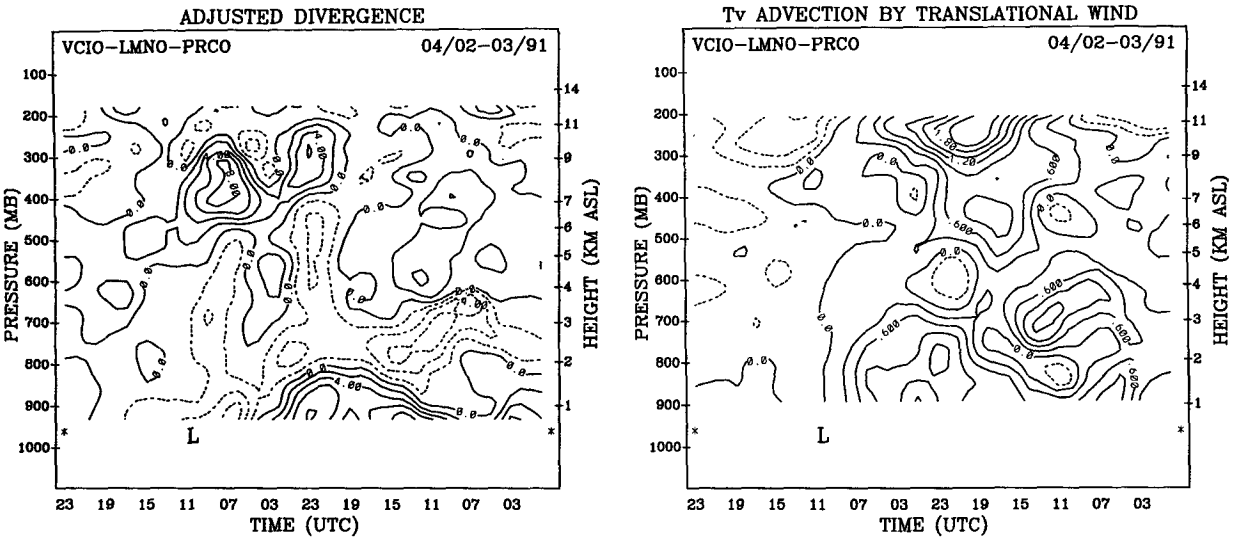

FIG. 8. *(Continued)*

that during the early morning hours of 2 April an upper-level ridge is traversing the network. At low levels, a strong low-level jet appears, as indicated by wind speeds of over 20 m s^{-1} in the lowest 100 mb between 0500 and 1100 UTC 2 April. Inspection of the first three moments of the Doppler power spectrum (signal power, radial velocity, and velocity variance), however, indicates the presence of migrating birds below 3 km AGL from 0300 to 1100 UTC 2 April (M. Ralph 1994, personal communication). [Wilczak et al. (1995) and Mclaughlin (1993) provide discussions of bird interference on WPDN data.] Therefore, the triangle calculations at low levels during this period are not reliable. However, sounding data and NMC 700-mb analyses (not shown) do indicate the presence of forcing for rising motion via warm thermal advection during the morning hours of 2 April, which is consistent with the band of clouds forming over central and western sections of Oklahoma (Fig. 5). During the afternoon of 2 April, subsidence (Fig. 8d) begins to dominate at V–L–P, especially at low levels, where lower-tropospheric divergence decreases rapidly with height (Fig. 8e), allowing for clearing skies in the western portions of the state.

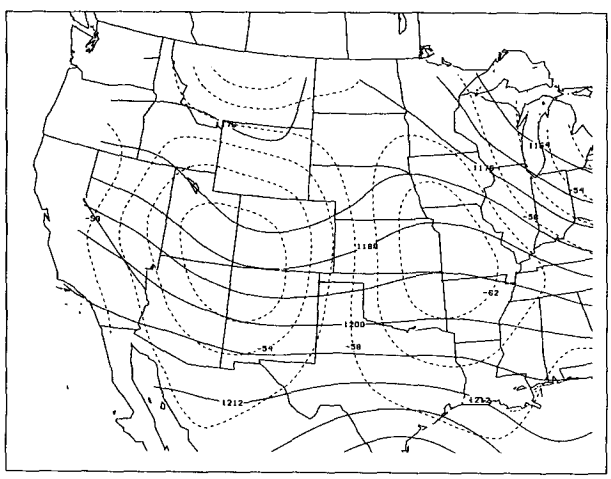

FIG. 9. GEMPAK analysis of 200-mb heights (dam, solid lines; contour interval of 6 dam) and temperature (°C, dashed lines; contour interval of 2°C) for 1200 UTC 2 April 1991.

Since the surface low and southward-extending dryline remain just west of Oklahoma during this time, low-level moisture continues to be advected into the western half of the state by strong southeasterly winds. Thus, there is a region in western Oklahoma where skies are mostly clear with a moist boundary layer becoming destabilized by solar heating, conditions that Carr and Millard (1985) showed are favorable for "dry-slot convection." Recall that the translational wind field reveals that a trough is approaching V–L–P, but at the time of the initiation of the dry-slot convection (around 1900 UTC), this trough is nearly 12 hours upstream. Therefore, the forcing associated with this trough is well to the west of the dryline. However, a close examination of the Purcell profiler data (Fig. 11) reveals a rather subtle feature: a trough embedded within southwesterly flow ahead of the major trough axis (near 2300 UTC 2 April between 700 and 400 mb).

Derivative fields show the presence of this embedded wave particularly well. The V–L–P vorticity time–height series (Fig. 8b) shows the passage of an upper-level vorticity maximum at 2300 UTC 2 April. The divergence field (Fig. 8e) near the time of the initiation of the convection shows a region of divergence near 300 mb that is associated with the smaller wave. This

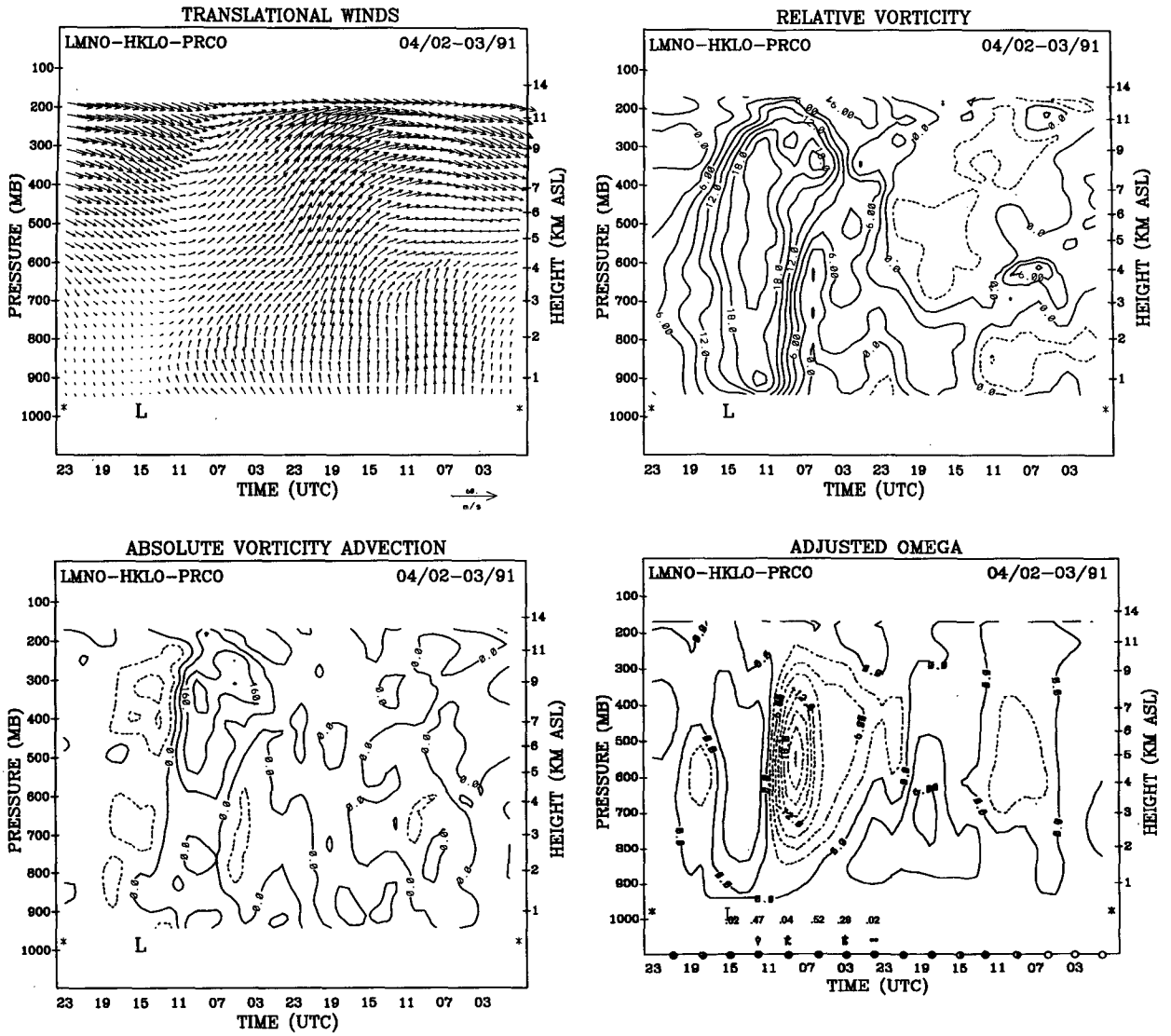

FIG. 10. Same as Fig. 4 except for the LMNO–HKLO–PRCO triangle for 2–3 April 1991. Weather information on Fig. 10d is for TUL, which lies near the eastern edge of the triangle.

upper-tropospheric divergence (and the associated positive DCVA inferred from Fig. 8c and mid- and upper-tropospheric rising motion) helps provide an environment conducive for the dry-slot convection. [Doswell (1987) provides discussion concerning the roles of large-scale and mesoscale contributions to severe convection.] Divergence and sinking motion prevail in the lower troposphere during the latter hours of 2 April at V–L–P (Figs. 8e and 8d, respectively). However, farther west, low-level mesoscale convergence along the dryline (Fig. 12) provides sufficient lift to initiate the convection (Figs. 5 and 7).

One important issue to address is the relationship between the dry-slot convection and the associated derived upper-tropospheric features. Convection can be initiated in areas influenced by *preexisting* perturbations in flow patterns (e.g., upper-level divergence), but studies indicate that convection can actually *cause* upper-level perturbations. For example, Maddox (1980) found that upper-level flow fields can respond to and be modified by persistent thunderstorm complexes. The results of Fankhauser (1974) suggest that "upper tropospheric divergence, long considered a prognostic indicator of severe thunderstorms may at times be a result and not necessarily the precursor of organized convective activity."

Considering that the upper-level feature and the dry-slot convection appear over the triangle at about the same time and that the short-wave trough went unde-

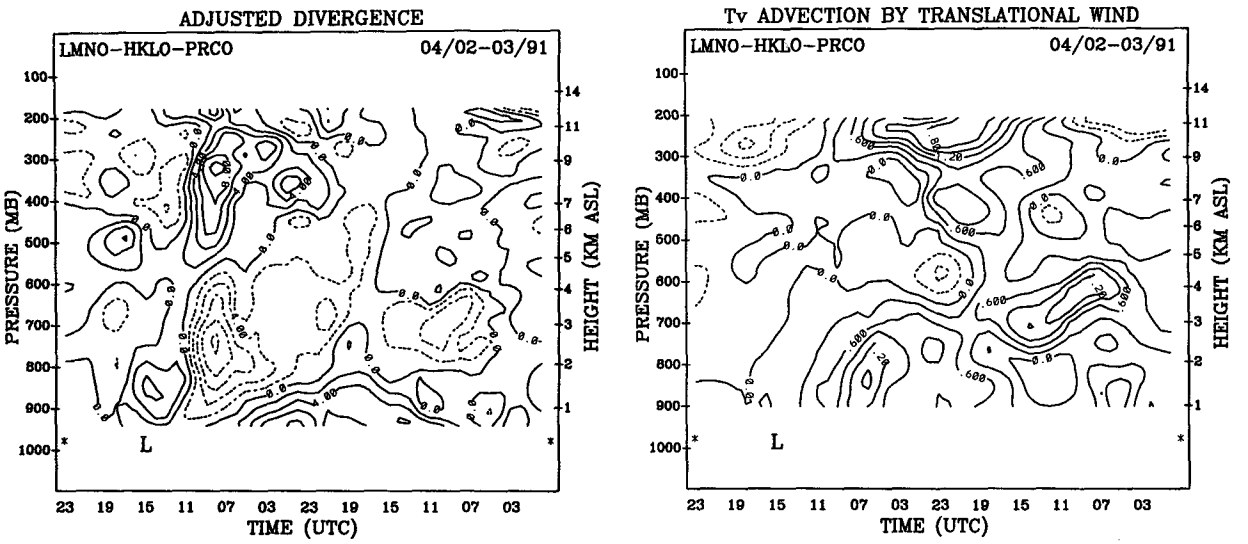

FIG. 10. (*Continued*)

tected by the rawinsonde network, we are unable to determine *conclusively* the relationship between the convection and the upper-level subsynoptic-scale trough, that is, whether the trough helps condition the environment for convection or whether the convection perturbs the upper flow such that those features seen in Fig. 8 near 2300 UTC 2 April are *produced.* Profiler data in the Texas panhandle showing the existence of the wave prior to the onset of convection might provide an answer to this dilemma. Unfortunately, such data are not available. However, since convective complexes are divergent at the upper levels, it is unlikely that the upper-level vorticity shown in Fig. 8b is convectively generated. Therefore, based on this consideration, we believe that the upper-level feature associated with the dry-slot convection is not merely a product of the convection itself but is a factor in conditioning the environment for convection.

6. Summary and concluding remarks

In this study, we have used wind profiler data to investigate the kinematic and thermodynamic structure of an amplifying and a decaying baroclinic wave, both

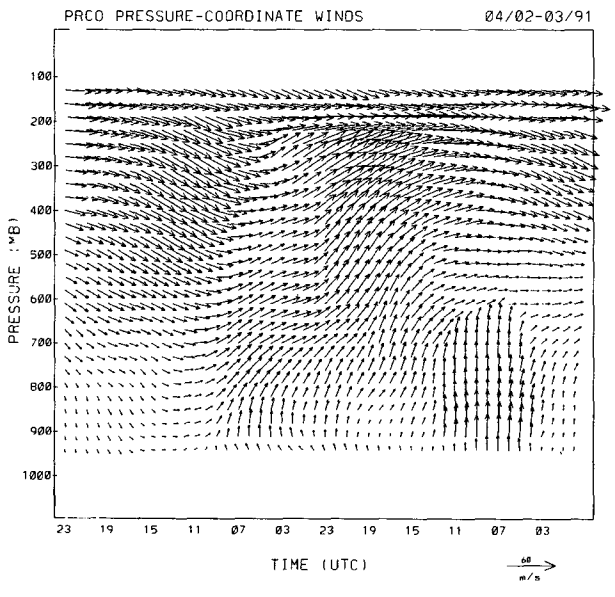

FIG. 11. PRCO pressure-coordinate winds for 2–3 April 1991.

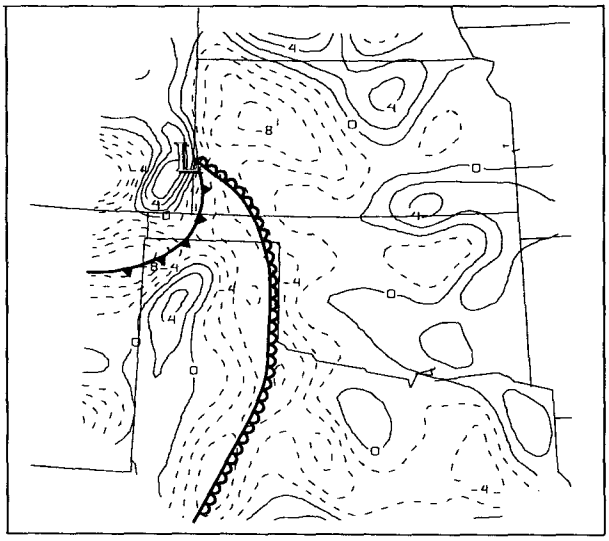

FIG. 12. GEMPAK surface convergence analysis ($\times 10^5$; contour interval of 2 s^{-1}) for 1900 UTC 2 April 1991. Dashed contours indicate convergence.

of which were associated with a severe convective episode. We found that the distribution of the profiler-derived kinematic and thermodynamic quantities relative to the surface low are indeed consistent with conceptual models of vertically tilted systems. In particular, advective processes contributing to cyclogenesis (cyclonic vorticity advection increasing with height and upper-level warm thermal advection) were present over the surface low during the amplification phase of the 7–8 October 1992 system, while those advective patterns contributing to cyclolysis (cyclonic vorticity advection decreasing with height and upper-level cold thermal advection) were present over the surface low during the decaying phase of the 2–3 April 1991 system. In the latter case, those advective patterns favoring cyclogenesis change to patterns favoring cyclolysis as the upstream-tilted trough transforms to a downstream-tilted trough.

While these particular results are not surprising, it is encouraging to see how the hourly nature of profiler data can provide forecasters with vital information on temporal scales not resolved by the operational rawinsonde network. For example, even in the midst of our diagnosis of tilted troughs, we ourselves were surprised to see that the profiler network captured a subsynoptic-scale wave embedded within southwesterly flow ahead of the 2–3 April 1991 major trough axis, while the rawinsonde network gave no indication of its presence.

Neimann and Shapiro (1989) found that "profiler-retrieved thermal . . . advections . . . compared favorably with those observed by the operational rawinsonde network." Karyampudi et al. (1995) used profiler data to diagnose a descending mesoscale tropopause fold and related the associated increase in absolute vorticity to a cyclogenetic event in the lee of the Rockies. Our application of profiler-derived thermal advection patterns (derived using a simple thermal wind equation) focused on the relationship between the phase of the upper-level patterns and the surface low evolution. These studies show that profiler winds can be used to accurately diagnose (at least qualitatively) mesoscale thermal processes.

The calculations for the decaying wave show that significant changes in the kinematic and thermodynamic structure of the major trough axis occurred as it passed through adjacent triangles whose centroids are only 100 km apart. Future work will begin to examine kinematic and thermodynamic properties of shortwave troughs using the *entire* network of wind profilers.

Finally, as useful as the profiler data are becoming, these datasets are by no means able to replace the current rawinsonde network that exists over the United States. Profiler data provide a *supplement* to the data that are currently available to forecasters. However, the usefulness and importance of wind profiler technology is underscored as more investigations using these fascinating new datasets are completed.

Acknowledgments. The authors express their gratitude to Dave Stensrud for his many helpful criticisms and suggestions. We thank Howie Bluestein for reviewing an earlier version of the text. Thanks also to Steve Million, Keith Brewster, and Jim Ladue for helping provide the data and to Harold Brooks and Joan O'Bannon for assisting with some of the figures. We also thank the two anonymous reviewers whose constructive comments improved the content and presentation of the manuscript. This research was supported in part by Grant ATM-8819619 from the National Science Foundation.

REFERENCES

Augustine, J. A., and E. J. Zipser, 1987: The use of wind profilers in a mesoscale experiment. *Bull. Amer. Meteor. Soc.*, **68,** 4–17.

Barth, M. F., R. B. Chadwick, and D. W. van de Kamp, 1994: Data processing algorithms used by NOAA's wind profiler demonstration network. *Ann. Geophys.*, **12,** 518–528.

Boyle, J. S., and L. F. Bosart, 1986: Cyclone–anticyclone couplets over North America. Part II: Analysis of a major cyclone event over the eastern United States. *Mon. Wea. Rev.*, **114,** 2432–2465.

Brewster, K. A., and T. W. Schlatter, 1986: Automated quality control of wind profiler data. Preprints, *11th Conf. on Weather Forecasting and Analysis,* Kansas City, KS, Amer. Meteor. Soc., 171–176.

Carlson, C. A., and G. S. Forbes, 1989: A case study using kinematic quantities derived from a triangle of VHF Doppler wind profilers. *J. Atmos. Oceanic Technol.*, **6,** 769–778.

Carr, F. H., and J. P. Millard, 1985: A composite study of comma clouds and their association with severe weather over the Great Plains. *Mon. Wea. Rev.*, **113,** 370–387.

——, P. L. Spencer, C. A. Doswell III, and J. D. Powell, 1995: A comparison of two objective analysis techniques for profiler time–height data. *Mon. Wea. Rev.*, **123,** 2165–2180.

Cram, J. M., M. L. Kaplan, C. A. Mattocks, and J. W. Zack, 1991: The use and analysis of profiler winds to derive mesoscale height and temperature fields: Simulation and real data experiments. *Mon. Wea. Rev.*, **119,** 1040–1056.

Davies-Jones, R., 1993: Useful formulas for computing divergence, vorticity, and their errors from three or more stations. *Mon. Wea. Rev.*, **121,** 713–725.

Doswell, C. A., III, 1977: Obtaining meteorologically significant surface divergence fields through the filtering property of objective analysis. *Mon. Wea. Rev.*, **105,** 885–892.

——, 1987: The distinction between large-scale and mesoscale contribution to severe convection: A case study example. *Wea. Forecasting,* **2,** 3–16.

——, and F. Caracena, 1988: Derivative estimation from marginally sampled vector point functions. *J. Atmos. Sci.*, **45,** 242–253.

Fankhauser, J. C., 1974: The derivation of consistent fields of wind and geopotential height from mesoscale rawinsonde data. *J. Appl. Meteor.*, **13,** 637–646.

Gage, K. S., and B. B. Balsley, 1978: Doppler radar probing of the clear atmosphere. *Bull. Amer. Meteor. Soc.*, **59,** 1074–1093.

Hermes, L. G., 1991: Comparisons of rawinsonde-deduced kinematic and thermodynamic quantities with those deduced from VHF profiler observations. *Mon. Wea. Rev.*, **119,** 1693–1712.

Hirschberg, P. A., and J. M. Fritsch, 1991: Tropopause undulations and the development of extratropical cyclones. Part I: Overview and observations from a cyclone event. *Mon. Wea. Rev.*, **119,** 496–517.

Holton, J. R., 1992: *An Introduction to Dynamic Meteorology,* 3d ed. Academic Press, 511 pp.

Karyampudi, V. M., M. L. Kaplan, S. E. Koch, and R. J. Zamora, 1995: The influence of the Rocky Mountains on the 13–14 April

1986 severe weather outbreak. Part I: Mesoscale lee cyclogenesis and its relationship to severe weather and dust storms. *Mon. Wea. Rev.*, **123,** 1394–1422.

Koch, S. E., M. DesJardins, and P. J. Kocin, 1983: An interactive Barnes objective map analysis scheme for use with satellite and conventional data. *J. Climate Appl. Meteor.*, **22,** 1487–1503.

Kuo, Y-H., D. O. Gill, and L. Cheng, 1987: Retrieving temperature and geopotential fields from a network of wind profiler observations. *Mon. Wea. Rev.*, **115,** 3146–3165.

Larsen, M. F., and J. Röttger, 1982: VHF and UHF Doppler radars as tools for synoptic research. *Bull. Amer. Meteor. Soc.*, **63,** 996–1008.

Lee, J. L., and G. L. Browning, 1994: Analysis of errors in the horizontal divergence derived from high temporal resolution of the wind. *Mon. Wea. Rev.*, **122,** 851–863.

Maddox, R. A., 1980: An objective technique for separating macroscale and mesoscale features in meteorological data. *Mon. Wea. Rev.*, **108,** 1108–1121.

Mclaughlin, S. A., 1993: Potential errors in Doppler radar wind measurements caused by migrating point targets as seen by the ARL FM-CW radar. Preprints, *26th Int. Conf. on Radar Meteorology,* Norman, OK, Amer. Meteor. Soc., 643–645.

Neiman, P. J., and M. A. Shapiro, 1989: Retrieving horizontal temperature gradients and advections from single-station wind profiler observations. *Wea. Forecasting,* **4,** 222–233.

——, P. T. May, and M. A. Shapiro, 1992: Radio acoustic sounding system (RASS) and wind profiler observations of lower- and midtropospheric weather systems. *Mon. Wea. Rev.*, **120,** 2298–2313.

Petterssen, S., 1956: *Weather Analysis and Forecasting (Vol. I). Motion and Motion Systems.* McGraw-Hill, 428 pp.

Schaefer, J. T., and C. A. Doswell III, 1979: On the interpolation of a vector field. *Mon. Wea. Rev.*, **107,** 458–476.

Shapiro, M. A., T. Hample, and D. W. van de Kamp, 1984: Radar wind profiler observations of fronts and jet streams. *Mon. Wea. Rev.*, **112,** 1263–1266.

Strauch, R. G., D. A. Merritt, K. P. Moran, K. B. Earnshaw, and D. van de Kamp, 1984: The Colorado wind-profiling network. *J. Atmos. Oceanic Technol.*, **1,** 37–49.

——, B. L. Weber, A. S. Frisch, C. G. Little, D. A. Merritt, K. P. Moran, and D. C. Welsh, 1987: The precision and relative accuracy of profiler wind measurements. *J. Atmos. Oceanic Technol.*, **4,** 563–571.

Weber, B. L., and D. B. Wuertz, 1990: Comparison of rawinsonde and wind profiler radar measurements. *J. Atmos. Oceanic Technol.*, **7,** 157–174.

——, ——, R. G. Strauch, D. A. Merritt, K. P. Moran, D. C. Law, D. van de Kamp, R. B. Chadwick, M. H. Ackley, M. F. Barth, N. L. Abshire, P. A. Miller, and T. W. Schlatter, 1990: Preliminary evaluation of the first NOAA demonstration network wind profiler. *J. Atmos. Oceanic Technol.*, **7,** 909–918.

Wilczak, J. M., and Coauthors, 1995: Contamination of wind profiler data by migrating birds: Characteristics of corrupted data and potential solutions. *J. Atmos. Oceanic Technol.*, **12,** 449–467.

Zamora, R. J., M. A. Shapiro, and C. A. Doswell III, 1987: The diagnosis of upper-tropospheric divergence and ageostrophic wind using profiler wind observations. *Mon. Wea. Rev.*, **115,** 871–884.

——, B. L. Weber, and D. C. Welsh, 1994: The accuracy of divergence estimates calculated using the linear vector point function method and three profilers. *Mon. Wea. Rev.*, **122,** 2603–2606.